ChemPubSoc Europe

DOI: 10.1002/chem.201702113

CHEMISTRY A European Journal Full Paper

Supramolecular Chemistry |*Hot Paper*|

Tuning the Porphyrin Building Block in Self-Assembled Cages for Branched-Selective Hydroformylation of Propene

Xiaowu Wang[+],[a, c] Sandra S. Nurttila[+],[a] Wojciech I. Dzik,[a] René Becker,[a] Jody Rodgers,[b] and Joost N. H. Reek*[a]

Abstract: Unprecedented regioselectivity to the branched aldehyde product in the hydroformylation of propene was attained on embedding a rhodium complex in supramolecular assembly **L2**, formed by coordination-driven self-assembly of tris(*meta*-pyridyl)phosphine and zinc(II) porpholactone. The design of cage **L2** is based on the ligand-template approach, in which the ligand acts as a template for cage formation. Previously, first-generation cage **L1**, in which zinc(II) porphyrin units were utilized instead of porpholactones, was reported. Binding studies demonstrate that the association constant for the formation of second-generation cage **L2** is nearly an order of magnitude higher than that of **L1**. This strengthened binding allows cage **L2** to remain intact in polar and industrially relevant solvents. As a consequence, the unprecedented regioselectivity for branched aldehyde products can be maintained in polar and coordinating solvents by using the second-generation assembly.

Introduction

Transition metal catalysis provides powerful tools for the selective construction of chemical bonds and thus is important for the development of sustainable and economical routes to chemicals.[1–6] The traditional approach in transition metal catalysis involves the optimization of catalyst properties by modifying the ligands that are coordinated to the active metal center. Typical properties of ligands that have proven influential include electronic[7] and steric effects[7] as well as bite angle.[8] More recently, it has been recognized that ligands that partake in the catalytic event can also be useful to invoke new reactivity.[9] Enzymes, nature's catalysts, can be very efficient and selective, and thus have been a source of inspiration for scientists. Whereas this inspiration initially resulted in systems in which substrate binding sites were connected to catalytic centers,[10] more recent strategies have explored placing catalysts in confined spaces. This leads to systems in which selectivity can be controlled by the second coordination sphere, that is, the supramolecular cage surrounding the active site. To date most examples of cage-controlled catalysis involve organic transformations, such as acyl transfer reactions,[11] Diels–Alder reactions,[12–15] imine-forming reactions,[16] hydrolysis reactions,[17,18] photoinduced rearrangements,[19] and cyclization reactions.[20] More recently, metal-catalyzed reactions carried out in molecular cages were also disclosed.[10,21–23] For example, encapsulation of a gold(I) phosphine complex in a supramolecular host resulted in an eightfold increase in the catalytic activity for hydroalkoxylation of allenes.[24] The same host was also capable of encapsulating a cationic Ir^{III} half-sandwich complex that was active in the C–H activation of aldehydes and exhibited both substrate-size and substrate-shape selectivity.[25] The effects of confinement have also been studied in hydrogenation and hydroformylation reactions. By encapsulation of an Rh^{I} norbornadiene complex in a self-folding cavitand, a hydrogenation catalyst capable of reducing norbornadiene was obtained.[26] Interestingly, a large difference in product selectivity between the encapsulated and free catalyst was observed, whereby the free catalyst favored dimer formation, whereas the encapsulated catalyst predominantly formed norbornene. By utilizing monophosphane rhodium complexes trapped inside cyclodextrins, highly branched selective and enantioselective hydroformylation of styrene could be achieved.[27] Moreover, cyclodextrins have been employed as reverse phase-transfer catalysts allowing hydrogenation of unsaturated alcohols[28] and hydroformylation of water-insoluble olefins[29,30] in aqueous media. Further examples of cage catalysis include

[a] *Dr. X. Wang,[+] S. S. Nurttila,[+] Dr. W. I. Dzik, Dr. R. Becker, Prof. Dr. J. N. H. Reek*
Van't Hoff Institute for Molecular Sciences, University of Amsterdam
Science Park 904, 1098 XH Amsterdam (The Netherlands)
E-mail: j.n.h.reek@uva.nl

[b] *Dr. J. Rodgers*
Eastman Chemical Company
P.O. Box 7444, Longview, TX 75607-7444 (USA)

[c] *Dr. X. Wang[+]*
Present address: Qingdao Institute of Bioenergy and Bioprocess Technology, Chinese Academy of Sciences
No. 189 Songling Road, Laoshan District, Qingdao 266101 (P. R. China)

[+] *These authors contributed equally to this work.*

Supporting information and the ORCID identification number for the author of this article can be found under https://doi.org/10.1002/chem.201702113.

gold(I)-catalyzed cyclization of acetylenic acid to enol lactone[26] and cobalt(II)-catalyzed radical-type cyclopropanation.[27] One of the challenges in the approach used in the above examples is that, at least for part of the catalytic cycle, the metal complex and the substrate must be co-encapsulated, which is challenging, particularly in the presence of excess substrate and product.[22] In addition, it is essential that no competing reaction pathways take place outside the cage. Although it has been demonstrated that this is possible in some cases, and leads to interesting examples of cage-controlled activity and selectivity, it is also clear that this is not a general strategy. We previously introduced a more general strategy to encapsulate catalysts in an efficient way that involves a ligand-template approach to encapsulate catalytically active metal centers. The key is that the catalyst is noncovalently linked to the surrounding cage, and thereby the strategy is applicable to a variety of catalytic systems.[28] The first example that we reported along these lines was **L1,** which was formed by the assembly of three Zn^{II} *meso*-tetraphenylporphyrins (Zn^{II}TPP) around the ligand template tris(*meta*-pyridyl)phosphine [P(*m*-py)$_3$] through selective N–Zn coordinate bonding. The phosphorus atom located in the center of the cage defined by the three porphyrins is available for metal coordination (Figure 1).

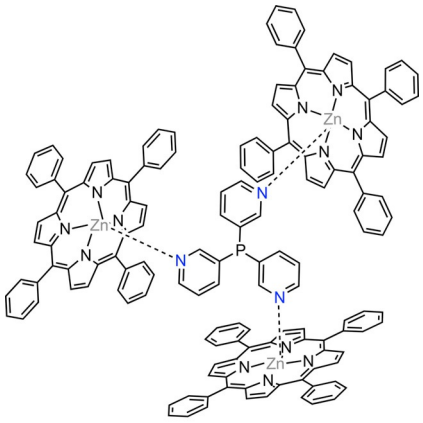

L1

Figure 1. First-generation assembly **L1** formed by the self-assembly of P(*m*-py)$_3$ and three equivalents of Zn^{II}TPP.

By coordination of the central phosphine ligand to rhodium, efficient hydroformylation catalysts[28,29] were obtained (Scheme 1). In the rhodium-catalyzed hydroformylation of 1-octene, encapsulation resulted in a tenfold increase in catalytic activity. Remarkably, preferential formation of the branched aldehyde product was observed (linear-to-branched ratio (l/b) = 0.6; room temperature). This unusual selectivity was ascribed to the encapsulation of the catalytically active species in the cavity defined by the three porphyrins.

The ligand-template approach was further extended to asymmetric hydroformylation of internal alkenes.[30,31] Here, bulky, chiral pyridine-based phosphoramidite ligands were used in combination with zinc(II) templates for the formation of encapsulated rhodium(I) catalysts. The encapsulated catalysts outperformed their non-supramolecular analogues in both activity and enantioselectivity. Furthermore, the ligand-template approach has been employed in many other ligand systems, such as BIAN, xanthene phosphine, and hybrid bidentate ligands, which demonstrate the strength and generality of this specific approach.[23,32–34]

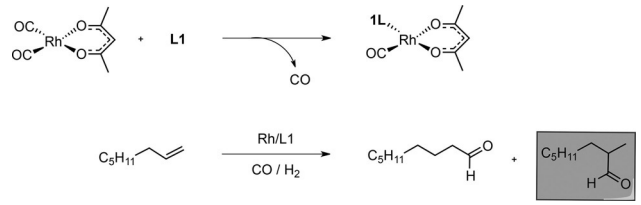

Scheme 1. Coordination of the central phosphine in assembly **L1** to rhodium(I) leads exclusively to encapsulated rhodium monophosphine complexes. When applied in 1-octene hydroformylation, selective formation of the branched aldehyde product was observed (l/b = 0.6).

All initial hydroformylation reactions were conducted at room temperature or slightly above, as the zinc–pyridine interaction was anticipated to be weaker at elevated temperatures. To extend the application window to more industrially relevant conditions, assembly **L1** was applied in 1-octene hydroformylation at temperatures as high as 75 °C.[35] Interestingly, the assembly retained its branched-aldehyde selectivity at higher partial pressures of CO. This demonstrates that, even though the interactions are weaker at elevated temperatures, the overall structure is thermodynamically sufficiently stable for cage-controlled catalysis.[36]

Because the zinc–pyridine interaction is strongest in apolar solvents, only noncoordinating solvents such as toluene and dichloromethane were employed. With increasing polarity or coordinating ability of the solvent, the binding constant of the zinc–pyridine interaction decreases, and this could potentially lead to a shift of the equilibrium to the non-encapsulated catalyst. However, from an industrial point of view it would be preferable to move away from toluene and chlorinated solvents, which have been listed as problematic in the CHEM21 solvent selection guide.[37] Many polar solvents, such as ketones, alcohols, and various esters, on the other hand, have been classified as industrially recommended solvents.

Hydroformylation of propene is currently performed in relatively polar solvents that potentially can coordinate to the zinc porphyrin unit in competition with the pyridyl group. We envisioned that, by modifying the cage-forming porphyrin in such a way that the strength of the zinc–pyridine interaction is increased, the use of the cage could be extended to more polar and industrially interesting solvents. Previously, we have shown that substituting the porphyrins at the phenyl group is only possible at one of the *meso* positions, as *para* and *ortho* substitution deformed the cage to a large extent.[29,38] Increasing the binding constant in this manner was only successful to a limited extent. This raises the question whether the binding strength can be increased by introducing modifications directly at the porphyrin ring.

In this contribution, we demonstrate that the zinc–pyridine binding constant of zinc(II) *meso*-tetraphenylporpholactone

(Zn^{II}TPPL) is nearly an order of magnitude higher compared to the parent Zn^{II}TPP. The resulting self-assembled cage retains the branched selectivity but can now also be applied in more polar, industrially relevant solvents. Importantly, as the modification is at the core of the porphyrin and no bulky substituents are introduced, cage formation is not disrupted.

Results and Discussion

Formation of the cage

To increase the stability of the supramolecular cage in polar and more competing solvents, we modified the porphyrin scaffold to strengthen the zinc–pyridine interaction. We chose Zn^{II}TPPL (TPPL = 5,10,15,20-tetraphenyl-8*H*-7-oxaporphyrin-8-one), an oxidized form of Zn^{II}TPP (TPP = 5,10,15,20-tetraphenylporphyrin), which was used in the first-generation cage **L1**. As such, the zinc center is more electron deficient, and we expected that this would result in a larger binding constant with pyridine in a variety of solvents. Zn^{II}TPPL is thermally stable and was obtained by direct oxidation of free-base *meso*-tetraphenylporphyrin (TPP-2H) and subsequent metalation in 30% overall yield (Scheme 2).[39]

On mixing P(*m*-py)$_3$ and three equivalents of Zn^{II}TPPL in toluene, assembly **L2** was formed by selective pyridine–zinc coordination (Scheme 3). The selective coordination of the pyridine groups of the phosphine to the zinc centers was confirmed by UV/Vis and NMR spectroscopy and a solid-state structure (vide infra).

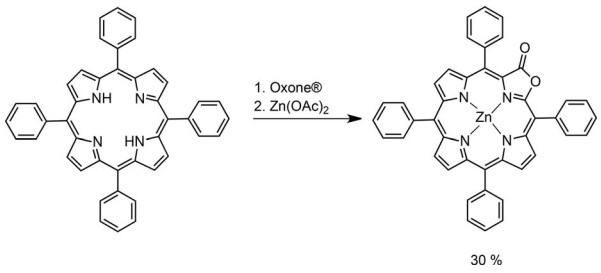

Scheme 2. Direct oxidation and subsequent metalation of TPP-2H to yield Zn^{II}TPPL.

Single crystals of sufficient quality for X-ray diffraction were grown by slow vapor diffusion of pentane into a solution of P(*m*-py)$_3$ and three equivalents of Zn^{II}TPPL in toluene at room temperature without taking precautions against air. The assembly crystallized as phosphine oxide adduct **L3** (Figure 2). The diffraction data allowed unambiguous assignment conformation of the cage, and confirmed the formation of a Zn^{II}TPPL-based assembly. The structures of **L3** and first-generation assembly **L1** are compared in Figure 2.

Previously, we reported the crystal structure of supramolecular assembly **L1**, in which all three porphyrin moieties are engaged in mutual CH–π interactions.[38] However, in the crystal structure of assembly **L3**, such CH–π interactions are present only between two porpholactone moieties that are tilted towards the axis passing through the P=O bond. This results in the environment around the phosphorus atom being more sterically congested compared to that of first-generation assembly **L1**. The Zn–N distances of assembly **L3** are 2.158(3) (Zn1–N1), 2.174(3) (Zn2–N2), and 2.182(3) (Zn3–N3). The different cavity shapes of assemblies **L1** and **L3** may be a result of different crystal packing forces, and as such these are not necessarily different in solution. Importantly, the average Zn–N distance of the Zn^{II}TPPL moiety to P(*m*-py)$_3$ is shorter than that of the Zn^{II}TPP moiety to P(*m*-py)$_3$, which points to stronger binding of pyridyl groups to Zn^{II}TPPL compared to Zn^{II}TPP.

Binding studies

To confirm our hypothesis that the binding affinity of pyridine to Zn^{II}TPPL is higher than of Zn^{II}TPP, we determined the 1:1 host–guest binding constants in various solvents by UV/Vis titration experiments (Table 1; for binding curves, see Supporting Information). On coordination of pyridine to Zn^{II}TPPL the typical redshift of both the Soret and the Q bands was observed in all used solvents: toluene, dichloromethane, acetone, and dioctyl terephthalate (DOTP).[40] All titration curves exhibited isosbestic points, indicating that a simple transition from one species (H = host) to another (HG = host–guest) takes place. All the titration curves fitted well with the typical equilibrium equation of a complex with 1:1 stoichiometry, from which the association constants were determined. As a typical example, overlapping absorption spectra and the titration

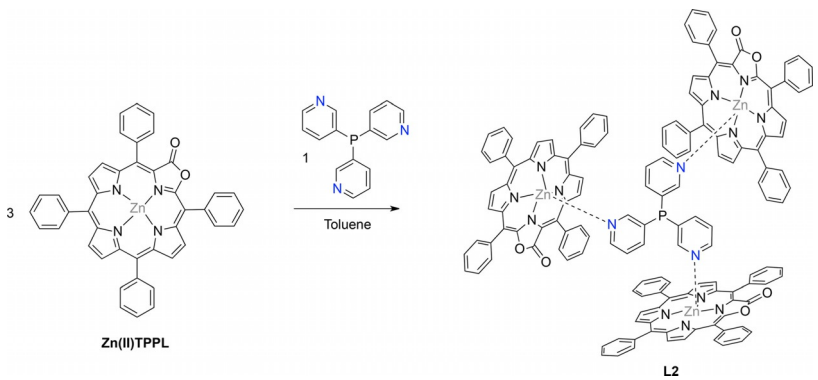

Scheme 3. Three equivalents of Zn^{II}TPPL and P(*m*-py)$_3$ assemble to form cage **L2** in toluene.

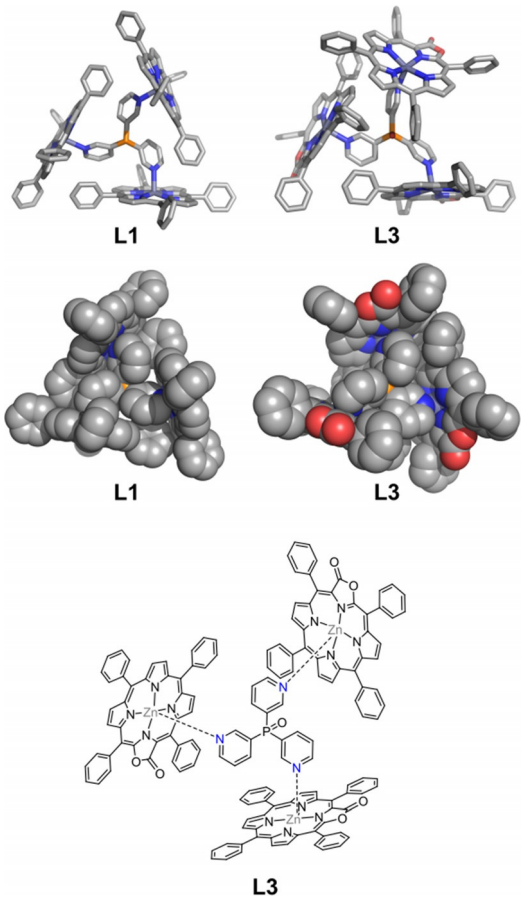

Figure 2. Comparison between the crystal structure of parent assembly **L1** and the new assembly **L3** as stick (top) and space-filling models (middle) and molecular structure (bottom) of the assembly. Solvent molecules and hydrogen atoms have been omitted for clarity. Color code: C, grey; N, blue; O, red; P, orange; Zn, purple.

Table 1. Association constants K for 1:1 binding of pyridine with Zn^{II}TPPL or Zn^{II}TPP in different solvents at 298 K.

Solvent	K_{ZnTPPL} [M^{-1}]	K_{ZnTPP} [M^{-1}]	K_{ZnTPPL}/K_{ZnTPP}
CH_2Cl_2	2.27×10^4	6.92×10^3	3.28
toluene	1.40×10^4	3.41×10^3	4.11
acetone	8.57×10^2	7.05×10^2	1.22
DOTP	1.02×10^3	2.98×10^2	3.42

curve for the 1:1 binding between Zn^{II}TPPL and pyridine in dichloromethane are shown in Figure 3a and b. The 1:1 stoichiometry for this specific binding event was further confirmed by Job plot analysis (see Supporting Information, Figures S23 and S24).

As expected, the binding constant of pyridine to Zn^{II}TPPL ($K=2.27\times10^4$ M^{-1}) is more than three times higher than that of Zn^{II}TPP when dichloromethane is used as solvent. In toluene this difference is even larger, although the absolute binding constant for the pyridine–Zn^{II}TPPL complex is slightly lower ($K=1.40\times10^4$ M^{-1}). Surprisingly, in acetone, the binding constants for pyridine to Zn^{II}TPP and Zn^{II}TPPL are almost identical, and slightly less than 1000. Interestingly, the binding constant

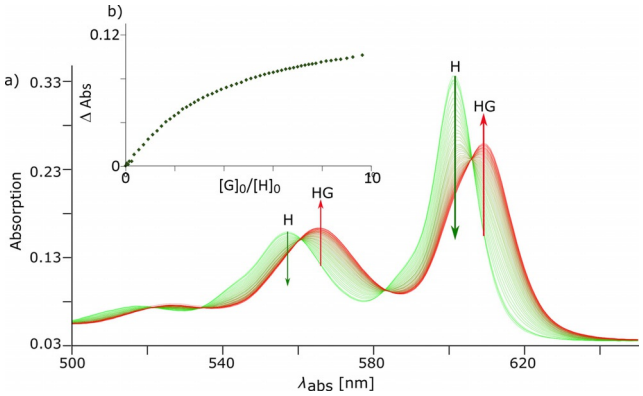

Figure 3. a) Overlay of UV/Vis spectra of the titration of Zn^{II}TPPL (host) with pyridine (guest) at a fixed host concentration of 16 μM in dichloromethane at 298 K. b) Absorption variation at the right Q band versus equivalents of added guest.

in a solvent that is industrially applied and is also rather polar, namely, DOTP, is more than three times higher for Zn^{II}TPPL compared to Zn^{II}TPP. Most importantly, the binding constant of pyridine to Zn^{II}TPPL in this solvent is only three times smaller than that of pyridine to Zn^{II}TPP in toluene, the conditions of the previously reported system. With these promising results in hand, we anticipated that cage-controlled catalysis would now also be possible in these more polar solvents (vide infra).

Next, the differences in the binding constants for the formation of cages **L1** and **L2** were investigated. Previously, it was reported that positive cooperativity plays a role in the formation of cage **L1**.[29] To investigate whether such an effect is present in the self-assembly of second-generation cage **L2**, 1:3 host–guest titrations were performed separately for assemblies **L1** and **L2**. The titration of **L1** was repeated to allow a valid comparison in which both sets of data are acquired and fitted with the same procedure. As UV/Vis spectroscopy turned out to be unsuitable for studying the 1:3 binding of the systems, ^{1}H and ^{31}P NMR spectroscopy was utilized instead (for further details regarding the challenges of using UV/Vis spectroscopy for studying 1:3 binding, see Supporting Information).

The use of NMR spectroscopy allowed us to monitor the changes in the signals of P(*m*-py)$_3$ on binding of Zn^{II}TPP and Zn^{II}TPPL. Importantly, by tracking the phosphine signals the supramolecular system can be saturated to the 1:3 complex, which we anticipated would allow us to further study the cooperativity in both systems. ^{1}H and ^{31}P NMR signals of the phosphine were monitored in parallel throughout the titration, and this resulted in more reliable data for the fitting procedures. In addition, the application of NMR spectroscopy permitted us to increase the absolute concentration of both the host and guest in solution, which led to more informative titration curves.

During the formation of assembly **L1**, upfield shifts of all four pyridine peaks in the ^{1}H NMR spectrum and the phosphorus peak in the ^{31}P NMR spectrum were observed. In the formation of assembly **L2** similar shifts were detected in the ^{1}H NMR spectrum; however, in the ^{31}P NMR spectrum the phosphine peak shifted downfield. These NMR shifts are as expected for

similar systems in the literature, and are caused by the anisotropic ring currents of the porphyrin/porpholactone moieties.[41,42] By fitting the ^{1}H and ^{31}P NMR titration curves simultaneously, binding constants for the formation of both assemblies could be derived (for binding curves, see Supporting Information). Interestingly, a positive cooperativity effect was found for both assemblies **L1** and **L2**, whereby the second and third binding event is stronger than the first one. The calculated binding constants are listed in Table 2 along with the cooperativity factors. For assembly **L2** a small cooperativity effect is present, but much less pronounced than for **L1**. This is in correspondence with the presence of fewer CH–π interactions in the crystal structure of **L2** compared to **L1**.

Table 2. Association constants *K* for 1:3 binding of P(*m*-py)$_3$ with Zn^{II}TPPL or Zn^{II}TPP in [D$_8$]toluene at 298 K.

Zn^{II}TPPL			Zn^{II}TPP		
α_1[a]	α_2[a]	K [M^{-1}]	α_1[a]	α_2[a]	K [M^{-1}]
1.2	1.2	1.51×10^{4}	2.8	4.8	2.50×10^{3}

[a] Cooperativity factors for binding of the second and third porphyrin/porpholactone unit; where $K_1=3K$; $K_2=\alpha_1 K$; $K_3=\alpha_2 K/3$.

Application of assemblies in hydroformylation of 1-octene

Once the new assembly **L2** was thoroughly characterized, we focused on investigating its catalytic performance in the hydroformylation of 1-octene (Scheme 4). In parallel the same

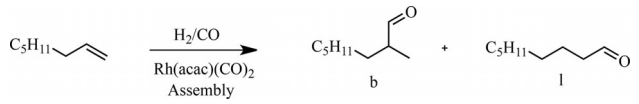

Scheme 4. Rhodium(I)-catalyzed hydroformylation of 1-octene.

catalytic reactions were performed with **L1**, to clearly study differences in activity and selectivity displayed by the first- and second-generation assemblies. 1-Octene is a benchmark substrate and an excellent model compound for tracking activity and selectivity of Rh^{I} hydroformylation catalysts.[3,43] Rhodium(I) complexes of the assemblies were generated in situ and used as such in catalysis. In all reactions five equivalents of assembly with respect to rhodium were used to avoid formation of active and nonselective ligand-free rhodium species. In all the reactions, a 1 h incubation time under syngas was applied before introduction of the substrate to allow complete formation of the Rh-coordinated assembly (for details of catalysis procedures, see Supporting Information). Reactions were carried out both at room temperature and at elevated, industrially relevant temperatures. The results for the hydroformylation of 1-octene are reported in Tables 3 and 4.

In the hydroformylation of 1-octene at room temperature, the first- and second-generation assemblies produced the product with nearly the same selectivity (see Table 3). Interestingly, the conversion of the substrate is twice as high for **L2** compared to **L1**, and this suggests that the activities are different. However, at higher temperatures the conversions are nearly identical. Both assembled catalysts maintain good selectivity for the branched aldehyde at a reaction temperature of 40 °C, and at 80 °C both catalyst systems lose their selectivity. This drop is expected and is due to the zinc–pyridine interaction becoming weaker at higher temperatures. We previously reported that, by increasing the partial pressure of CO in the gas mixture, higher selectivity for the branched aldehyde can be maintained with assembly **L1** at higher temperature.[35] Subsequent reactions were therefore carried out at elevated temperatures and pressures, and the effect of the CO concentration was investigated in more detail in the hydroformylation of propene (vide infra).

Table 3. Hydroformylation of 1-octene with Rh catalysts based on assemblies **L1** and **L2** at various temperatures in toluene.

Entry[a]	Assembly	*T* [°C]	Conv. [%]	TON	l/b
1	L1	25	10	440	0.56
2	L2	25	22	1080	0.60
3	L1	40	64	3130	0.84
4	L2	40	57	2760	0.89
5	L1	80	98	4100	1.97
6	L2	80	97	3720	2.22

[a] Reagents and conditions: 2 μmol (0.02 mol%) [Rh(acac)(CO)$_2$], 10 μmol (0.1 mol%) P(*m*-py)$_3$, 30 μmol (0.3 mol%) porphyrin/porpholactone, 0.01 mL DIPEA, 5.5 mL dry toluene, 20 bar H$_2$/CO (1:1), incubation time 1 h, reaction time 16–18 h.

Table 4. Hydroformylation of 1-octene with Rh-catalysts based on assemblies **L1** and **L2** at different solvents under industrially relevant conditions.

Entry[a]	Assembly	*T* [°C]	Solvent	Conv. [%]	l/b
1	**L1**	75	toluene	>99	0.78
2	**L2**	75	toluene	>99	0.99
3[b]	none	75	toluene	>99	1.72
4	**L1**	75	DOTP	>99	0.96
5	**L2**	75	DOTP	>99	1.08
6[b]	none	75	DOTP	>99	2.31
7	**L1**	75	acetone	10	1.12
8	**L2**	75	acetone	28	1.35
9[b]	none	75	acetone	58	1.75

[a] Reagents and conditions: 0.5 μmol (0.02 mol%) [Rh(acac)(CO)$_2$], 2.5 μmol (0.1 mol%) P(*m*-py)$_3$, 7.5 μmol (0.3 mol%) porphyrin/porpholactone, 0.002 mL DIPEA, 1.5 mL solvent, 80 bar H$_2$/CO (1:1), incubation time 1 h, reaction time 16–19 h. [b] No porphyrin/porpholactone was added; only P(*m*-py)$_3$ was used.

Next, the solvent scope of the reaction was evaluated in the hydroformylation of 1-octene, by using three different solvents at high temperature (75 °C) and pressure (80 bar) (Table 4). Due to the larger binding constant of pyridine to Zn^{II}TPPL in all solvents explored, we expected assembly **L2** to perform better in the more polar and industrially relevant solvents acetone and DOTP (see Figure 4). However, again assemblies **L1** and **L2** perform nearly equally well in all three solvents, although the selectivity is slightly higher for the first-generation assembly. In

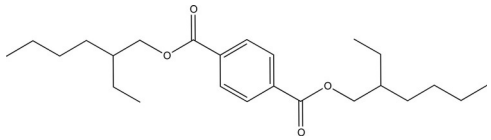

Figure 4. The structure of industrially relevant solvent dioctyl terephthalate.

all cases the cages outperform their non-encapsulated catalyst analogues showing that even at high temperatures the cages are mostly intact.

Application of assemblies in hydroformylation of propene

We next focused on the hydroformylation of the more challenging substrate propene (Scheme 5). The challenge lies in the small size of propene and the lack of directing functional groups, which generally result in relatively low selectivity for the branched aldehyde.

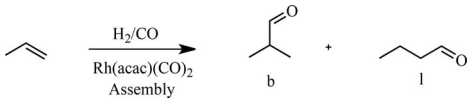

Scheme 5. Rhodium(I)-catalyzed hydroformylation of propene.

First, we evaluated the effect of the CO and H_2 partial pressures on the hydroformylation of propene, knowing that these parameters greatly affect both the activity and selectivity of 1-octene hydroformylation. We explored this effect for the first-generation assembly **L1**, for which the effect of CO concentration was earlier reported in the hydroformylation of 1-octene.[35] Thus, we could directly conclude whether the same effect is present for propene. The results are shown in Tables 5 and 6. As expected, an increase in the partial pressure of CO leads to higher selectivity for the branched aldehyde, whereas the activity and productivity of the catalyst decrease (Table 5, entries 1–4).

Remarkably, rather high selectivity (l/b = 1.12) was preserved at a temperature as high as 70 °C, and this clearly demonstrates the correlation between a high CO concentration and relatively strong preference for formation of the branched aldehyde in propene hydroformylation. The opposite effect is observed for an increase in the partial pressure of H_2, whereby the activity and productivity of the catalyst are increased at the cost of selectivity (Table 6). Similar effects are observed when performing catalysis at a set pressure of 20 bar while varying the CO/H_2 ratio (see Supporting Information, Table S1).

Having concluded that a high CO partial pressure is important for the branched selectivity, not only in 1-octene but also in propene hydroformylation, we explored the effect of temperature on the reaction with both assemblies. Second-generation assembly **L2** showed higher selectivity both at room temperature and at elevated temperatures (Table 7). To the best of our knowledge, this is the highest selectivity for the branched aldehyde product in propene hydroformylation reported to date. Interestingly, first-generation cage **L1** outperforms **L2** in benchmark 1-octene hydroformylation in terms of branched selectivity, whereas the opposite effect is observed in propene hydroformylation.

Table 5. Hydroformylation of propene with Rh catalysts based on assembly **L1** at different partial pressures of CO at 70 °C.

Entry[a]	Assembly	p_{H_2} [bar]	p_{CO} [bar]	p_{tot} [bar]	TON	TOF_{max}[b]	l/b
1	**L1**	12.5	12.5	25	7600	1500	1.40
2	**L1**	12.5	16.7	29.2	6370	950	1.30
3	**L1**	12.5	25	37.5	6180	880	1.20
4	**L1**	12.5	37.5	50	5610	690	1.12

[a] Reagents and conditions: 2 μmol $[Rh(acac)(CO)_2]$, 10 μmol P(*m*-py)$_3$, 30 μmol porphyrin, 0.01 mL DIPEA, 5.5 mL dry toluene, 8 bar propene, 70 °C, reaction time 16 h. [b] TOF_{max} = turnover frequency [mol mol^{-1} h^{-1}]; see Supporting Information for calculation of TOF_{max}.

Table 6. Hydroformylation of propene with Rh catalysts based on assembly **L1** at different partial pressures of H_2 at 70 °C.

Entry[a]	Assembly	p_{H_2} [bar]	p_{CO} [bar]	p_{tot} [bar]	TON	TOF_{max}[b]	l/b
1	L1	12.5	12.5	25	7600	1500	1.40
2	L1	16.7	12.5	29.2	9050	1840	1.44
3	L1	25	12.5	37.5	4940	4810	1.58
4	L1	37.5	12.5	50	11 500	6600	2.10

[a] Reagents and conditions: 2 μmol $[Rh(acac)(CO)_2]$, 10 μmol P(*m*-py)$_3$, 30 μmol porphyrin, 0.01 mL DIPEA (*N*,*N*-diisopropylethylamine), 5.5 mL dry toluene, 8 bar propene, 70 °C, reaction time 16 h. [b] TOF_{max} = turnover frequency [mol mol^{-1} h^{-1}]; see Supporting Information for calculation of TOF_{max}.

Table 7. Hydroformylation of propene with Rh catalysts based on assemblies **L1** and **L2** at various temperatures in toluene.

Entry[a]	Assembly	*T* [°C]	TON	TOF_{max}[b]	l/b
1	**L1**	25	390	60	0.94
2	**L2**	25	480	75	0.84
3	**L1**	70	5600	690	1.12
4	**L2**	70	5570	500	1.11

[a] Reagents and conditions: 2 μmol $[Rh(acac)(CO)_2]$, 10 μmol P(*m*-py)$_3$, 30 μmol porphyrin/porpholactone, 0.01 mL DIPEA, 5.5 mL dry toluene, 8 bar propene, 50 bar H_2/CO (1:3), reaction time 15–17 h. [b] TOF_{max} = turnover frequency [mol mol^{-1} h^{-1}]; see Supporting Information for calculation of TOF_{max}.

With these surprising results in hand, we attempted to find an explanation for the selectivity differences between the assemblies. The average Zn–N distance in assembly **L2** is shorter than that in **L1** in the solid state. Although in solution, the shape of the new assembly is likely dynamic, we assume that this difference in Zn–N distance may still play an important role in the catalytic performance. Preliminary volume calculations based on the crystal structures of **L1** and **L2** were carried out to shine light on the effect of going from Zn^{II}TPP to Zn^{II}TPPL on catalysis (for calculations, see Supporting Informa-

tion). Interestingly, the cavity volume of assembly **L2** is 44% smaller than that of **L1**. Thus, by exchanging a porphyrin for a porpholactone not only the binding strength, but also the size of the cage is changed. This could be a plausible explanation for the observed selectivity differences in catalysis. It is likely that a smaller cage is more selective in the conversion of the smaller propene, whereas the slightly larger capsule provides a more branched-selective hydroformylation catalyst for larger substrates such as 1-octene.

Finally, we carried out hydroformylation of propene with both assemblies in toluene and in the more competitive solvent DOTP under industrially relevant conditions (Table 8). Interestingly, assembly **L2** shows both higher activity and selectivity in more polar and coordinating solvent DOTP. This effect can be directly attributed to the larger binding constant of the zinc–pyridine interaction for assembly **L2** in DOTP. As hypothesized, an increase in the binding constant between zinc and pyridine allows for a more stable cage in polar solvents. By means of this small change in the cage-forming units, we have extended the branched-selective hydroformylation of propene to more industrially relevant conditions and solvents (DOTP). These results are consistent with **L2** being both smaller and more stable than cage **L1**.

Table 8. Hydroformylation of propene with Rh catalysts based on assemblies **L1** and **L2** in different solvents at 70 °C.

Entry[a]	Assembly	Solvent	TON	TOF_{max}[b]	l/b
1	**L1**	toluene	5600	690	1.12
2	**L2**	toluene	5570	500	1.11
3	**L1**	DOTP	1273	107	1.45
4	**L2**	DOTP	4130	167	1.28

[a] Reagents and conditions: 2 μmol $Rh(acac)(CO)_2$, 10 μmol P(*m*-py)$_3$, 30 μmol porphyrin/porpholactone, 0.01 mL DIPEA, 5.5 mL dry toluene, 8 bar propene, 50 bar H_2/CO (1:3), 70 °C, reaction time 17 h. [b] TOF_{max} = turnover frequency [mol mol^{-1} h^{-1}]; see Supporting Information for calculation of TOF_{max}.

Conclusions

This work describes the encapsulation of a rhodium complex in a supramolecular assembly based on P(*m*-py)$_3$ and Zn^{II}TPPL. The resulting supramolecular catalyst displays the highest selectivity for the branched aldehyde in the hydroformylation of propene (l/b = 0.84). In the current system, porpholactone units are used to generate the second coordination sphere around the active catalyst, whereas previously we have used normal Zn^{II}TPP. This small change in the electronics of the porphyrin has a large effect on the binding constant and as such also on the stability of the cage. In addition, X-ray analysis of the assembly shows that the cage volume is also slightly smaller. As a result of these differences, the new self-assembled cage gives unprecedented branched selectivity in the hydroformylation of propene, whereas the use of the cage based on Zn^{II}TPP gives higher branched selectivity for 1-octene. Importantly, the increased zinc–pyridine interaction observed for Zn^{II}TPPL allows the reaction to be performed in industrially relevant solvent DOTP while maintaining high selectivity in propene hydroformylation. Thus, we have demonstrated that making small changes to the building blocks of the assembly allows fine tuning of the catalyst properties such that these can be applied under industrially relevant conditions.

Experimental Section

General procedures

All reactions were carried out under an atmosphere of N_2 by using standard Schlenk techniques unless otherwise stated. CH_2Cl_2 was distilled from CaH_2 under N_2, and pentane and toluene were distilled from Na under N_2. NMR spectra were recorded with Bruker AMX 300 (300.1, 75.5, and 121.5 MHz for ^{1}H, ^{13}C, and ^{31}P, respectively), Bruker AMX 400 (400.1, 100.6, and 162.0 MHz for ^{1}H, ^{13}C, and ^{31}P, respectively), and Bruker AMX 500 (500.1, 125.8, and 202.5 MHz for ^{1}H, ^{13}C, and ^{31}P, respectively) spectrometers. $CDCl_3$ was used as solvent unless otherwise specified, and the ^{1}H NMR spectra were referenced to the residual solvent signal. ESI-MS measurements were recorded with a JEOL JMS SX/SX102A four-sector mass spectrometer, UV/Vis spectra were recorded with a Shimadzu UV-2000 spectrophotometer in a 10 mm quartz cuvette. Gas chromatographic analyses of 1-octene hydroformylation was performed with a Shimadzu GC-17A apparatus. Gas chromatographic analyses of propene hydroformylation was performed with a TRACE GC Ultra instrument (Thermo Electron Corporation) and a Shimadzu GC-17A instrument. Kinetic data were recorded with a Brooks 0254 instrument. X-ray diffraction data were collected with a Bruker D8 Quest Eco single-crystal diffractometer equipped with a CMOS Photon 50 detector by using Mo_{Ka} radiation. All reagents were purchased from commercial suppliers and used without further purification, unless otherwise noted. 1-Octene was filtered through basic alumina before use.

Single-crystal X-ray diffraction

$C_{144}H_{90}N_{15}O_7PZn_3 + 2\,C_7H_8$ + disordered solvent, FW = 2553.73 (derived values do not include the contribution of the disordered solvent), violet-red rough fragment, 0.32 × 0.20 × 0.11 mm, triclinic, $P\bar{1}$ (no. 2), a = 18.0306(10), b = 20.7321(12), c = 21.3054(12) Å, α = 95.628(3), β = 99.410(3), γ = 106.576(3), V = 7441.8(7) Å^3, Z = 2, ρ_{exptl} = 1.140 g cm^{-3} (derived values do not include the contribution of the disordered solvent), μ = 0.548 mm^{-1} (derived values do not include the contribution of the disordered solvent). In total, 203 052 reflections were measured with a Bruker D8 Quest Eco diffractometer, equipped with a TRIUMPH monochromator and a CMOS PHOTON 50 detector (λ = 0.71073 Å) up to a resolution of $(\sin\theta/\theta)_{max}$ = 0.83 Å^{-1} at 150(2) K. The intensity data were integrated with the Bruker APEX2 software.[44] Absorption correction and scaling were performed with SADABS.[45] (0.64–0.75 correction range). In total, 26 675 reflections were unique (R_{int} = 0.085), of which 19 584 were observed [$I > 2\sigma(I)$]. The structure was solved by direct methods with the program SHELXS-97[46] and refined with SHELXL-2013 against F^2 of all reflections. One of the porpholactone moieties is positionally disordered (rotation over a 90° axis) and the lactone moiety was refined as occupying two sites with occupancy factors of 0.64 and 0.36. The structure contains voids (1695 Å^3 per unit cell) filled with disordered solvent molecules. Their contribution to the structure factors was secured by back-Fourier transformation with the SQUEEZE routine of the PLATON package,[47] resulting in 226 electrons per unit cell. 1657 parameters were included in the least-squares refinement. Non-hydrogen atoms were re-

fined with anisotropic displacement parameters. Hydrogen atoms were introduced in calculated positions and refined with a riding model. $R1/wR2$ [$I > 2\sigma(I)$]: 0.0606/0.1751. $S = 1.020$. Residual electron density between −0.78 and 1.18 e Å^{-3}. Geometry calculations and checking for higher symmetry was performed with the PLATON program.[47]

Synthesis of *meso*-tetraphenyl-2-oxa-3-oxoporphyrinato zinc(II) (Zn^{II}TPPL)

Modified literature procedure[39,48]: Step 1: A solution of 2,2′-bipyridine (187.4 mg, 1.2 mmol, 0.5 equiv) in 1,2-dichloroethane (DCE, 20 mL) was added to a stirred mixture of 5,10,15,20-tetraphenylporphyrin (1.5 g, 2.4 mmol, 1 equiv) and $RuCl_3$ (248.9 mg, 1.2 mmol, 0.5 equiv) in DCE (750 mL) and water (750 mL), respectively. The solution was heated to 100 °C. A mixture of Oxone® (7.377 g, 12 mmol, 5 equiv) and NaOH (480 mg, 12 mmol, 5 equiv) was added in five portions over 5 h. The reaction was quenched with a saturated aqueous solution of $Na_2S_2O_3$, after which the organic layer was separated and the aqueous layer was extracted twice with dichloromethane. The combined organic layers were dried with Na_2SO_4, filtered, and concentrated under vacuum. The residue was purified by column chromatography (silica gel, eluent: CH_2Cl_2/hexane = 2:1) to give the product, 5,10,15,20-tetraphenylporpholactone, as a purple solid (yield 45%, 683.3 mg, 1.08 mmol). ^{1}H NMR (500 MHz, $CDCl_3$, 293 K): $\delta = 8.80$ (dd, $J = 5.0$, 1.7 Hz, 1H), 8.76 (dd, $J = 5.0$, 1.8 Hz, 1H), 8.70 (dd, $J = 4.9$, 1.7 Hz, 1H), 8.60 (d, $J = 4.9$ Hz,1H), 8.58 (dd, $J = 4.6$, 1.4 Hz, 1H), 8.53 (d, $J = 4.5$ Hz, 1H), 8.13 (m, 4H), 8.10 (m, 2H), 7.98 (m, 2H), 7.73 (m, 12H), −1.66 (s, 1H, NH), −2.03 (s, 1H, NH).

Step 2: 5,10,15,20-Tetraphenylporpholactone (290 mg, 0.458 mmol, 1 equiv) and $Zn(OAc)_2$ were suspended in $CHCl_3$/EtOH (2:1, 120 mL). The reaction mixture was heated to 70 °C for 2 h. Afterwards, the reaction mixture was cooled and filtered through Celite. The filtrate was concentrated and purified by column chromatography (silica gel, eluent: CH_2Cl_2, $R_f = 0.44$). The bright green band was collected and all the solvent was evaporated to afford a green purple solid in 80% yield (255 mg, 0.366 mmol). ^{1}H NMR (500 MHz, $CDCl_3$, 298 K): $\delta = 8.72$ (br s, 6H), 8.13 (br s, 6H), 7.8 (br s, 14H). Due to strong self-aggregation, the peaks are broad and cannot be assigned. For better resolution of peaks, 2 equiv of pyridine were added. ^{1}H NMR (500 MHz, $CDCl_3$, 298 K): ^{1}H NMR (500 MHz, $CDCl_3$, 293 K): $\delta = 8.74$ (d, $J = 4.7$ Hz, 1H, pyrrole-H), 8.66 (dd, $J = 7.3$ Hz, 4.6 Hz, 2H, pyrrole-H), 8.60 (d, $J = 4.5$ Hz, 1H, pyrrole-H), 8.54 (d, $J = 4.5$ Hz, 1H, pyrrole-H), 8.50 (d, $J = 4.5$ Hz, 1H, pyrrole-H), 8.10 (d, $J = 7.7$ Hz, 4H), 8.05 (d, $J = 6.7$ Hz, 2H, Ph-H), 7.93 (d, $J = 6.2$ Hz, 2H, Ph-H),7.70 (m, 12H, Ph-H), 7.17 (t, $J = 7.5$ Hz, 2H, *p*-Py), 6.58 (t, $J = 7.5$ Hz, 4H, *m*-Py), 5.93 (br s, 4H, *o*-Py).

Typical procedure for catalysis

In a flame-dried Schlenk vessel under N_2, metalloporphyrin (0.03 mmol), a stock solution of P(*m*-py)$_3$ (0.01 mmol) in toluene ($c = 0.026$ M), neat DIPEA (0.06 mmol),[49] a stock solution of [Rh(acac)(CO)$_2$] (0.002 mmol) in toluene ($c = 0.005$ M), and substrate were added consecutively. Toluene was added to the reaction mixture to reach the same total volume for all experiments. An autoclave was evacuated and flushed with N_2 three times. The above reaction mixture was transferred to the autoclave with a syringe and stainless steel needle (≈25 cm). The autoclave was then flushed three times with 20 bar syngas. Then the autoclave was pressurized to the required pressure, immersed in a preheated oil bath, and stirred at a fixed speed. After a preset reaction time, the reaction mixture was cooled and the pressure was carefully released. Tri-*n*-butyl phosphite (20 μL) was added to quench the active rhodium catalyst. A 10–20 μL aliquot of the reaction mixture was diluted to 1 mL with solvent and directly measured by GC without further workup.

Acknowledgements

We thank the Eastman Chemical Company and the European Research Council (ERC Adv. NAT-CAT Reek) for kind financial support.

Conflict of interest

The authors declare no conflict of interest.

Keywords: homogeneous catalysis · hydroformylation · porphyrinoids · rhodium · supramolecular chemistry

[1] C. C. C. Johansson Seechurn, M. O. Kitching, T. J. Colacot, V. Snieckus, *Angew. Chem. Int. Ed.* **2012**, *51*, 5062 – 5085; *Angew. Chem.* **2012**, *124*, 5150 – 5174.
[2] R. Noyori, *Nat. Chem.* **2009**, *1*, 5 – 6.
[3] R. Franke, D. Selent, A. Börner, *Chem. Rev.* **2012**, *112*, 5675 – 5732.
[4] B. Cornils, W. A. Herrmann, in *Applied Homogeneous Catalysis with Organometallic Compounds*, Wiley-VCH, Weinheim, **1996**.
[5] R. A. Sheldon, I. W. C. E. Arends, U. Hanefeld, in *Green Chemistry and Catalysis*, Wiley-VCH, Weinheim, **2007**.
[6] G. Rothenberg in *Catalysis*, Wiley-VCH, Weinheim, **2008**.
[7] C. A. Tolman, *Chem. Rev.* **1977**, *77*, 313 – 348.
[8] Z. Freixa, P. W. N. M. van Leeuwen, *Dalton Trans.* **2003**, 1890 – 1901.
[9] J. Love, *Dalton Trans.* **2016**, *45*, 15700 – 15701.
[10] C. J. Brown, F. D. Toste, R. G. Bergman, K. N. Raymond, *Chem. Rev.* **2015**, *115*, 3012 – 3035.
[11] L. G. Mackay, R. S. Wylie, J. K. M. Sanders, *J. Am. Chem. Soc.* **1994**, *116*, 3141 – 3142.
[12] M. Marty, Z. Clyde-Watson, L. J. Twyman, M. Nakash, J. K. M. Sanders, *Chem. Commun.* **1998**, 2265 – 2266.
[13] C. J. Walter, H. L. Anderson, J. K. M. Sanders, *J. Chem. Soc. Chem. Commun.* **1993**, 458 – 460.
[14] J. Kang, G. Hilmersson, J. Santamaría, J. Rebek, *J. Am. Chem. Soc.* **1998**, *120*, 3650 – 3656.
[15] M. Yoshizawa, M. Tamura, M. Fujita, *Science* **2006**, *312*, 251 – 254.
[16] T. Iwasawa, R. J. Hooley, J. Rebek, *Science* **2007**, *317*, 493 – 496.
[17] M. D. Pluth, R. G. Bergman, K. N. Raymond, *Science* **2007**, *316*, 85 – 88.
[18] J. L. Bolliger, A. M. Belenguer, J. R. Nitschke, *Angew. Chem. Int. Ed.* **2013**, *52*, 7958 – 7962; *Angew. Chem.* **2013**, *125*, 8116 – 8120.
[19] D. M. Dalton, S. R. Ellis, E. M. Nichols, R. A. Mathies, F. D. Toste, R. G. Bergman, K. N. Raymond, *J. Am. Chem. Soc.* **2015**, *137*, 10128 – 10131.
[20] D. M. Kaphan, F. D. Toste, R. G. Bergman, K. N. Raymond, *J. Am. Chem. Soc.* **2015**, *137*, 9202 – 9205.
[21] P. Dydio, J. N. H. Reek, *Chem. Sci.* **2014**, *5*, 2135 – 2145.
[22] S. H. A. M. Leenders, R. Gramage-Doria, B. de Bruin, J. N. H. Reek, *Chem. Soc. Rev.* **2015**, *44*, 433 – 448.
[23] T. S. Koblenz, J. Wassenaar, J. N. H. Reek, *Chem. Soc. Rev.* **2008**, *37*, 247 – 262.
[24] Z. J. Wang, C. J. Brown, R. G. Bergman, K. N. Raymond, F. D. Toste, *J. Am. Chem. Soc.* **2011**, *133*, 7358 – 7360.
[25] D. H. Leung, D. Fiedler, R. G. Bergman, K. N. Raymond, *Angew. Chem. Int. Ed.* **2004**, *43*, 963 – 966; *Angew. Chem.* **2004**, *116*, 981 – 984.
[26] M. A. Sarmentero, H. Fernández-Pérez, E. Zuidema, C. Bo, A. Vidal-Ferran, P. Ballester, *Angew. Chem. Int. Ed.* **2010**, *49*, 7489 – 7492; *Angew. Chem.* **2010**, *122*, 7651 – 7654.
[27] M. Jouffroy, R. Gramage-Doria, D. Armspach, D. Sémeril, W. Oberhauser, D. Matt, L. Toupet, *Angew. Chem. Int. Ed.* **2014**, *53*, 3937 – 3940; *Angew. Chem.* **2014**, *126*, 4018 – 4021.

[28] J. Potier, A. Guerriero, S. Menuel, E. Monflier, M. Peruzzini, F. Hapiot, L. Gonsalvi, *Catal. Commun.* **2015**, *63*, 74 – 78.
[29] T. Mathivet, C. Méliet, Y. Castanet, A. Mortreux, L. Caron, S. Tilloy, E. Monflier, *J. Mol. Catal. A* **2001**, *176*, 105 – 116.
[30] M. T. Reetz, S. R. Waldvogel, *Angew. Chem. Int. Ed. Engl.* **1997**, *36*, 865 – 867; *Angew. Chem.* **1997**, *109*, 870 – 873.
[31] Q.-Q. Wang, S. Gonell, S. H. A. M. Leenders, M. Dürr, I. Ivanović-Burmazović, J. N. H. Reek, *Nat. Chem.* **2016**, *8*, 225 – 230.
[32] M. Otte, P. F. Kuijpers, O. Troeppner, I. Ivanović-Burmazović, J. N. H. Reek, B. de Bruin, *Chem. Eur. J.* **2014**, *20*, 4880 – 4884.
[33] V. F. Slagt, J. N. H. Reek, P. C. J. Kamer, P. W. N. M. van Leeuwen, *Angew. Chem. Int. Ed.* **2001**, *40*, 4271 – 4274; *Angew. Chem.* **2001**, *113*, 4401 – 4404.
[34] V. F. Slagt, P. C. J. Kamer, P. W. N. M. van Leeuwen, J. N. H. Reek, *J. Am. Chem. Soc.* **2004**, *126*, 1526 – 1536.
[35] R. Bellini, S. H. Chikkali, G. Berthon-Gelloz, J. N. H. Reek, *Angew. Chem. Int. Ed.* **2011**, *50*, 7342 – 7345; *Angew. Chem.* **2011**, *123*, 7480 – 7483.
[36] R. Bellini, J. N. H. Reek, *Eur. J. Inorg. Chem.* **2012**, 4684 – 4693.
[37] R. Gramage-Doria, R. Bellini, J. Rintjema, J. N. H. Reek, *ChemCatChem* **2013**, *5*, 1084 – 1087.
[38] J. Flapper, J. N. H. Reek, *Angew. Chem. Int. Ed.* **2007**, *46*, 8590 – 8592; *Angew. Chem.* **2007**, *119*, 8744 – 8746.
[39] T. S. Koblenz, H. L. Dekker, C. G. de Koster, P. W. N. M. van Leeuwen, J. N. H. Reek, *Chem. Commun.* **2006**, 1700 – 1702.
[40] T. Besset, D. W. Norman, J. N. H. Reek, *Adv. Synth. Catal.* **2013**, *355*, 348 – 352.
[41] A. Satake, Y. Kobuke, *Tetrahedron* **2005**, *61*, 13 – 41.
[42] N. R. Babij, E. O. McCusker, G. T. Whiteker, B. Canturk, N. Choy, L. C. Creemer, C. V. De Amicis, N. M. Hewlett, P. L. Johnson, J. A. Knobelsdorf, F. Li, B. A. Lorsbach, B. M. Nugent, S. J. Ryan, M. R. Smith, Q. Yang, *Org. Process Res. Dev.* **2016**, *20*, 661 – 667.
[43] V. Bocokić, A. Kalkan, M. Lutz, A. L. Spek, D. T. Gryko, J. N. H. Reek, *Nat. Commun.* **2013**, *4*, 2670.
[44] Y. Yu, H. Lv, X. Ke, B. Yang, J.-L. Zhang, *Adv. Synth. Catal.* **2012**, *354*, 3509 – 3516.
[45] M. Nappa, J. S. Valentine, *J. Am. Chem. Soc.* **1978**, *100*, 5075 – 5080.
[46] R. J. Abraham, G. R. Bedford, B. Wright, *Org. Magn. Reson.* **1982**, *18*, 45 – 52.
[47] I. Jacobs, A. C. T. van Duin, A. W. Kleij, M. Kuil, D. M. Tooke, A. L. Spek, J. N. H. Reek, K. Hermansson, *Catal. Sci. Technol.* **2013**, *3*, 1955 – 1963.
[48] P. W. N. M. van Leeuwen, C. Claver, in *Rhodium Catalyzed Hydroformylation (Catalysis by Metal Complexes)*, Kluwer, Dordrecht, **2000**.
[49] Bruker, APEX2 software, Madison, WI, USA, **2014**.
[50] SAINT, version 6.02, and SADABS, version 2.03, Bruker AXS, Inc., Madison, WI, **2002**.
[51] G. M. Sheldrick, *Acta Crystallogr. Sect. A* **2008**, *64*, 112 – 122.
[52] A. L. Spek, *Acta Crystallogr. Sect. D* **2009**, *65*, 148 – 155.
[53] T. C. Eisenschmid, G. A. Miller, R. R. Peterson, A. G. Abatjoglou, *Hydroformylation process with improved control over product isomers* (Dow Technology Investments), US20100069680, **2010**.
[54] DIPEA was used to neutralize potential traces of acid to prevent demetalation of ZnTPP. In a separate experiment it was confirmed that DIPEA had no influence on the catalysis results.

Manuscript received: May 10, 2017
Accepted manuscript online: June 13, 2017
Version of record online: August 17, 2017

